

Tracing shocks and photodissociation in the Galactic center region

Sergio Martín

*Harvard-Smithsonian Center for Astrophysics, 60 Garden St., 02138, Cambridge, MA,
USA*

smartin@cfa.harvard.edu

M.A. Requena-Torres

Max-Planck-Institut für Radioastronomie, Auf dem Hügel 69, D-53121 Bonn, Germany

J. Martín-Pintado

*Departamento de Astrofísica Molecular e Infrarroja, Instituto de Estructura de la Materia,
CSIC, Serrano 121, E-28006 Madrid, Spain*

R. Mauersberger

*Instituto de Radioastronomía Milimétrica, Avenida Divina Pastora 7, Local 20, E-18012
Granada, Spain*

ABSTRACT

We present a systematic study of the HNC O , C ^{18}O , ^{13}CS , and C ^{34}S emission towards 13 selected molecular clouds in the Galactic center region ¹. The molecular emission in these positions are used as templates of the different physical and chemical processes claimed to be dominant in the circumnuclear molecular gas of galaxies. The relative abundance of HNC O shows a variation of more than a factor of 20 among the observed sources. The HNC O / ^{13}CS abundance ratio is highly contrasted (up to a factor of 30) between the shielded molecular clouds mostly affected by shocks, where HNC O is released to gas-phase from grain mantles, and those pervaded by an intense UV radiation field, where HNC O is photo-dissociated and CS production favored via ion reactions. We propose the relative HNC O to CS abundance ratio as a highly contrasted diagnostic tool to distinguish between the influence of shocks and/or the radiation field in the nuclear regions of galaxies and their relation to the evolutionary state of their nuclear star formation bursts.

¹Based on observations carried out with the IRAM 30-meter telescope. IRAM is supported by INSU/CNRS (France), MPG (Germany) and IGN (Spain).

Subject headings: Galaxy: center — Galaxy: abundances — ISM: molecules — astrochemistry — galaxies: ISM

1. Introduction

The central few hundred parsecs of many galaxies, including our own, harbor large amounts of molecular gas and are the sites of past, present or future star formation. The interaction of the gas with the gravitational potential in such areas, with the radiation and outflows from recently formed and evolved stars, and with the central objects makes that the physical processes influencing this molecular gas are much more complex than in disk clouds. These physical processes not only dominate the energy balance in the circumnuclear environment of galaxies, but they also determine if stars could be formed within such clouds. In the central 300 pc of our own galaxy we find giant molecular clouds (GMC) harboring regions of massive star formation and heavily affected by shocks (Martín-Pintado et al. 2001); large regions where molecular gas is pervaded by intense UV photodissociating radiation (PDRs) stemming from massive star clusters (Krabbe et al. 1995; Figer et al. 1999; Rodríguez-Fernández et al. 2001); strong X-ray emission (Sidoli et al. 2001, and references therein) as well as the ultimate massive black hole candidate (Eisenhauer et al. 2005; Ghez et al. 2005). This variety of energetic processes not only modifies the distribution, kinematics, density and temperature of the gas but also drives different types of chemistry in the molecular gas in the Central Molecular Zone (CMZ, Morris & Serabyn 1996).

Comparing the chemical composition between Galactic regions with known dominant heating mechanisms can be used to trace the heating mechanisms in the central region of galaxies. Unbiased spectral line surveys of selected regions within our Galaxy allow to identify the different chemical signatures which trace the different dominant heating mechanisms affecting the nuclear interstellar medium (ISM) in galaxies with different type of activity and/or in different evolutionary states (Martín et al. 2006b).

One of the molecules whose abundance appears to be a particularly unambiguous tracer of shock heating is HNC. This asymmetric rotor has been observed in high mass molecular hot cores with fractional abundances relative to H_2 of $\sim 10^{-9}$ (Zinchenko et al. 2000) as well as in translucent and dark clouds with similar abundances (Turner et al. 1999). The observations of HNC toward the photodissociation regions in the Orion bar shows abundances of $\lesssim 1.6 \times 10^{-11}$ (Jansen et al. 1995), indicating this molecule is easily destroyed by the UV radiation. Within the Galactic center region, the low resolution C^{18}O (which is thought to be a tracer of the total H_2 column density) and HNC maps by Dahmen et al. (1997) as well as the close up view towards the Sgr A region by Lindqvist et al. (1995) clearly show

differences in their distribution which can not be ascribed to only differences in excitation but to real differentiation in the chemical properties of the different molecular complexes in the Milky Way. Minh & Irvine (2006) have mapped the Sgr B2 region and they identified an expanding ring-like structure in the HNC O emission, clearly different from that of ^{13}CO and HCO^+ . This suggests that HNC O is likely enhanced by the shock interaction between the expanding ring and the main cloud. Similar chemical differences in the distribution of the HNC O emission have also been observed at larger scales towards external galaxies (Meier & Turner 2005). Therefore HNC O seems to be a potential good tracer of different heating mechanisms in the nuclei of galaxies. However, there is not a systematic study of the physical conditions and the relative abundances of HNC O in a sample of molecular clouds in the CMZ affected by different type of heating mechanisms.

In this paper we present systematic multitransition observations of HNC O toward 13 molecular clouds in the Galactic center which are thought to be affected by different processes such as shocks, UV radiation, and X-rays. We explore the potential of HNC O to be used as a chemical discriminator of the different physical processes affecting the chemistry of the ISM. We show that the HNC O abundance ratio with respect to C^{18}O , ^{13}CS , and C^{34}S is an excellent discriminator between the molecular clouds affected by the UV radiation and moderate shocks. The proposed CS vs HNC O diagnostic diagram can be used to trace these type of activities in the extragalactic ISM.

2. Observations and Results

The observations were carried out with the IRAM 30 m telescope on Pico Veleta, Spain. The thirteen sources observed throughout the Galactic center region are shown in Table 1, where both the coordinates and the Galactic center complex where each source is located are given. During the observation we switched the position of the telescope between the source and a reference every 60 seconds. As reference positions we used $l = 0.65$, $b = 0.2$ ($\alpha_{\text{J2000}} = 17^{\text{h}}46^{\text{m}}23^{\text{s}}.0$, $\delta_{\text{J2000}} = -28^{\circ}16'37''$) for the sources in the Sgr B complex and $l = -0.25$, $b = -0.25$ ($\alpha_{\text{J2000}} = 17^{\text{h}}46^{\text{m}}00^{\text{s}}.1$, $\delta_{\text{J2000}} = -29^{\circ}16'47''$) for those around Sgr A in order to minimize the distances between source and reference for the sake of baseline stability. No significant emission was found in these reference positions when previously observed in frequency switched mode tuned to the frequencies of the CS $J = 3 - 2$ and $J = 5 - 4$ transitions at 146.9 and 244.9 GHz, respectively.

We observed the transitions of C^{18}O , C^{34}S , ^{13}CS and HNC O indicated in Tables 2 and 3. We have also observed the HNC ^{18}O $J=7_{0,7}-6_{0,6}$ line at 145.5 GHz in two positions with large HNC O column densities to estimate the opacity of the HNC O line. The SIS receivers

were tuned to SSB with image band rejections typically larger than 10 dB. At the observed frequencies the beamwidths of the telescope were 22'' (3 mm), 16'' (2 mm) and 10'' (1.3 mm). As spectrometers we used the 512×1 MHz filter bank for the 3 mm transition and the 256×4 MHz filter banks for the 2 and 1.3 mm lines.

Fig 1 show a sample of spectra where the brightest among the observed transitions of each species have been selected for each source. While single Gaussian profiles were fitted to most of the observed transitions, two Gaussians have been fitted to those sources showing asymmetric line profiles. The resulting integrated intensities and the radial velocities derived from the Gaussian fits are shown in Table 2 for the $C^{18}O$, $C^{34}S$ and ^{13}CS transitions and in Table 3 for those of HNC O .

We have derived the column density and excitation temperature by assuming that the excitation of all molecules is in local thermodynamic equilibrium (LTE), the lines are optically thin and the source is extended as compared to the telescope beam (see Goldsmith & Langer 1999; Martín et al. 2006b, for a detailed discussion on rotational diagrams). We do not detect emission for the HNC ^{18}O $J=7_{0,7}-6_{0,6}$ line to a limit of < 30 mK. Thus, for the typical $^{16}O/^{18}O$ ratio of 250 (Wilson & Rood 1994), the observed HNC O lines appear to be optically thin. In fact the $^{16}O/^{18}O$ ratio we derived for the Sgr B2 ($-40, 0$) position is > 300 , larger than the canonical value of 250. Fig 2 shows the rotational diagrams derived for three typical sources, namely a hot core, Sgr B2N, a GC molecular cloud, Sgr B2M($20'', 100''$), and a PDR in the circumnuclear disk (CND), Sgr A*. Rotational temperatures (T_{rot}) derived from $C^{18}O$ and $C^{34}S$ are similar for all the sources, with average values of 10.3 ± 1.9 K and 12 ± 3 K, respectively. Thus, we assumed a $T_{rot} = 10$ K to derive the ^{13}CS column densities. On the other hand, HNC O shows a wider range of rotational temperatures from 10 K up to 56 K. However, for most of the sources in the GC we derive values of $T_{rot} \sim 10$ K. Only the hot cores like Sgr B2 M, N, and S and the gas associated with photo dissociation regions (see Sec. 3.2) show larger T_{rot} . In fact, the HNC O diagrams of Sgr B2 N and M are fitted by a two gas component with temperatures of ~ 20 K, similar to the average found in the other sources, and ~ 100 K, typical of the hot cores. From the obtained rotational temperatures we have derived column densities shown in Table 4.

Fig. 3 shows the abundances of $C^{34}S$, ^{13}CS and HNC O relative to H_2 , where a $C^{18}O/H_2$ conversion factor of 1.7×10^{-7} has been assumed (Frerking et al. 1982). We note that the CS isotopologues show similar abundances for all the sources with changes smaller than a factor of 4 among all the observed sources. The $C^{34}S/^{13}CS$ ratio is also constant within a factor of 2.4 for all the sources except for the hot core Sgr B2N and G+0.18 – 0.04. Nevertheless, the non-detection of $C^{34}S$ in G+0.18 – 0.04 implies a surprisingly low abundance of this isotopical substitution in this source. The upper limit to the $C^{34}S/^{13}CS$ ratio of ~ 0.5 is a

factor of 3 below the average ratio derived for the other positions, suggesting a significant underabundance of ^{34}S in G+0.18 – 0.04 with respect to ^{13}CS .

3. Relative HNCO and ^{13}CS abundances

CS has been commonly used as a tracer of gas typically 100 times denser than that traced by CO ($n > 10^4 \text{ cm}^3$, Mauersberger & Henkel 1989; Mauersberger et al. 1989; McQuinn et al. 2002). The main precursor for the formation of CS in gas phase is S^+ (through chain reactions forming CS^+ and HCS^+ , Drdla et al. 1989). Therefore, even if photodissociation is the main mechanism of CS destruction, this molecule is observed to survive in regions with high UV radiation field, likely due to an enhancement of S^+ (with predicted abundances up to $\sim 10^{-5} \text{ cm}^{-3}$, Sternberg & Dalgarno 1995). In fact, CS has been used to estimate the abundance of the observationally elusive S^+ in PDRs (Goicoechea et al. 2006).

HNCO may trace material even denser than CS ($n_{\text{H}_2} \gtrsim 10^6 \text{ cm}^{-3}$; Jackson et al. 1984). The presence of HNCO in the icy grain mantles, though not directly observed, is suggested by the detection of OCN^- , which is thought to be produced by the reaction on grains between HNCO and NH_3 (Novozamsky et al. 2001, and references therein). Though HNCO can be formed via gas phase reactions (Iglesias 1977; Turner et al. 1999), its formation in solid phase seems to be more efficient (Hasegawa & Herbst 1993). The observed correlation of the HNCO emission with that of SiO in high mass star forming molecular cores suggests that HNCO abundance in gas phase is enhanced by grain erosion and/or disruption by shocks (Zinchenko et al. 2000). This correlation is also suggested for the Galactic center clouds from the maps of SiO and HNCO towards the Sgr A region (Minh et al. 2005).

In this work we did not use the emission from the main isotopologue of CS to avoid possible effects due to line opacity. Instead, we have used the $\text{HNCO}/^{13}\text{CS}$ as a diagnostic ratio which should be basically unaffected by opacity effects (Hüttemeister et al. 1998). As mentioned, the HNCO emission is also optically thin.

From Fig. 3, we notice that whenever the relative abundance of HNCO is higher than average, that of ^{13}CS tends to be lower than average and viceversa. In fact, the $\text{HNCO}/^{13}\text{CS}$ or $\text{HNCO}/\text{C}^{34}\text{S}$ ratios show much larger variations than the relative abundance variation of either of the molecules involved. This large differentiation in the HNCO abundance is clearly evidenced in Fig. 4, where we show the abundance ratio of $\text{HNCO}/^{13}\text{CS}$ versus the H_2 column density. The $\text{HNCO}/^{13}\text{CS}$ ratio varies by more than one order of magnitude between different sources. As for the $\text{HNCO}/\text{C}^{34}\text{S}$ ratios we found the same variations in the $\text{HNCO}/^{13}\text{CS}$ ratios. Most of this variation is due to the HNCO and only to a lesser degree

to CS.

From the HNC $\text{O}/^{13}\text{CS}$ abundance ratios in Fig. 4 we can clearly observe that the sources are clustered in three different categories, (described in detail below): a) Galactic center molecular clouds, represented as filled squares, showing moderate H_2 column densities with a high HNC $\text{O}/^{13}\text{CS}$ abundance ratio, b) PDRs shown as filled circles and high velocity shocks as open squares with a low HNC $\text{O}/^{13}\text{CS}$ abundance ratio, and c) hot cores, filled triangles, with larger H_2 column densities and intermediate HNC $\text{O}/^{13}\text{CS}$ abundance ratios.

3.1. Typical Galactic center clouds

The typical Galactic center clouds, hereafter “*giant molecular clouds*” (GMCs), are observed to have sizes of ~ 30 pc, densities around 10^{-4} cm^{-3} , and kinetic temperatures ≥ 80 K. These sources do not show any traces of recent or ongoing star formation activity (Güsten et al. 1981; Hüttemeister et al. 1993; Martín-Pintado et al. 1997). We find the largest HNC $\text{O}/^{13}\text{CS}$ abundance ratios towards the set of sources representative of these typical Galactic center GMCs (filled squares in Fig. 4). This group of sources includes the offset positions $(20'', 100'')$ and $(20'', -180'')$ in the molecular envelope of Sgr B2M, G+0.24 + 0.01, G−0.11 − 0.08, and G+0.83 − 0.18. Though located in very different environments and separated by more than 100 pc within the Galactic center region, all these GMCs share very similar relative abundances of HNC O to CS. We find a mean HNC $\text{O}/^{13}\text{CS}$ abundance ratio of 68 ± 13 for these sources.

The large abundances of complex molecules and of SiO in these molecular clouds are thought to be due to shocks, which eject these species from grain surfaces. These shocks must have a sufficiently low velocity to guarantee that the molecules are not dissociated (Hüttemeister et al. 1998; Martín-Pintado et al. 2001; Requena-Torres et al. 2006). Similarly, the large abundance of HNC O observed in this work towards these positions can be well explained by gas-phase injection via dust grain erosion by shocks in the molecular clouds across the Galactic center. Further support to this idea comes from the observations towards six sources common to those observed in this paper which show enhanced $\text{CH}_3\text{OH}/\text{CS}$ abundance ratios by a factor of ~ 25 , while the CS/H_2 ratio remains unchanged (Requena-Torres et al. 2006).

3.2. Photodissociation regions

We also observe a group of sources with a relative $\text{HNCO}/^{13}\text{CS}$ abundance ratio smaller by more than an order of magnitude than the values observed in the typical GMCs. This is the case of the observed position in the CNB around Sgr A* and the source G+0.18 – 0.04 (Filled dots in Fig. 4). These two sources (hereafter “*PDR clouds*”) are both located in the vicinity of massive star clusters and therefore are known to be the best candidates for a chemistry driven by the UV radiation from the stellar clusters.

The Sgr A* observed position is located in the CNB, ~ 1.5 pc (assuming a distance of ~ 8 Kpc to the GC) away from the nominal position of Sgr A*, and it is thus strongly pervaded by the UV radiation from the Central Cluster (Krabbe et al. 1995). G+0.18 – 0.04, in the region known as “the Sickie”, is strongly irradiated by the OB stars in the Quintuplet Cluster (Figer et al. 1999; Rodríguez-Fernández et al. 2001). The difference of a factor of ~ 3 in the $\text{HNCO}/^{13}\text{CS}$ abundance ratios observed between the two velocity components at 20 and 70 km/s^{-1} (the two leftmost filled dots in Fig. 4) are likely attributed to different degrees of UV irradiation due to the different spatial distribution of each component (Serabyn & Güsten 1991).

In extreme conditions with strong UV radiation field in the surroundings of the GC massive star clusters, the photo-resistant CS is expected to survive (Goicoechea et al. 2006), while the easily photodissociated HNCO molecule will quickly disappear from the gas phase as we get close to the source of UV radiation. In fact, HNCO is observed to be less resistant to the UV radiation than other easily dissociated molecules such as CH_3OH (Requena-Torres et al. 2006), also efficiently formed and ejected from dust grains (Millar et al. 1991; Charnley et al. 1995).

In addition to the previous sources, we observe another cloud with also very low $\text{HNCO}/^{13}\text{CS}$ abundance ratio, namely the position G+0.02 – 0.02. This object is a very compact cloud thought to be the result of the acceleration, heating and compression of the gas by a series of supernovae shocks (Oka et al. 1999). Irradiation by stellar UV photons is unlikely both due to the absence of free-free radio continuum emission associated with this cloud and the fact that it is too far to be illuminated by the Central Cluster. The radiative precursor associated with the J-type shocks resulting from the supernovae events which produces a significant UV radiation field (Shull & McKee 1979) might be a likely explanation to the observed low $\text{HNCO}/^{13}\text{CS}$ abundances ratios. In this scenario the dissociation of HNCO by the UV radiation generated in the shock would be equivalent to that observed in PDRs.

The average $\text{HNCO}/^{13}\text{CS}$ ratio for this group of sources is 5 ± 2 in the PDR clouds, more than one order of magnitude smaller than the average value measured in GC clouds. However,

for the best candidate of a PDR cloud, located in the CND, the measured abundance ratio $\text{HNCO}/^{13}\text{CS}$ is more than 20 times smaller than in the GC clouds. Our observations therefore indicate that the abundance ratio between the photo-resistant CS molecule and the shock injected fragile HNCO molecule is a powerful tool to discriminate between molecular material heavily affected by a PDR chemistry (PDR clouds) and that largely shielded from the UV radiation.

3.3. Hot cores and supernova interaction

Finally, we find a third group of sources which shows $\text{HNCO}/^{13}\text{CS}$ abundance ratios below those observed in GMCs but still significantly higher than those in PDR clouds. We observe in Fig. 4 that all these sources have H_2 column densities (as derived from C^{18}O) larger by a factor of 5, than those in the two groups previously discussed. These sources are hot molecular cores, namely Sgr B2 N, M and S, as well as the sources G–0.02 – 0.07 and Sgr B2 M ($-40'', 0''$). The Sgr B2 M ($-40'', 0''$) position is known to be associated with the ridge of a very recent massive star formation site detected by de Vicente et al. (2000). At this position, the detection of HC_3N vibrationally excited emission clearly shows the presence of hot cores like Sgr B2R4 associated with massive protostar like those found in Sgr B2M, N and S. The $\text{HNCO}/^{13}\text{CS}$ ratio in this position should therefore be dominated by the hot cores.

We derive fractional abundances of HNCO of $(5 \pm 2) \times 10^{-9}$ for the hot cores in our sample. The HNCO abundance observed by Zinchenko et al. (2000) in massive star forming regions, ranged from 2.5×10^{-9} , similar to our measurements, down to 2×10^{-10} . Our data confirm that HNCO appears to be underabundant towards hot molecular cores and that the largest abundances are not found toward the site of massive star formation. From the maps of HNCO towards G301.12-0.20 and G270.26+0.83 (Zinchenko et al. 2000), one observes that the HNCO emission does not peak at the IRAS position, though position uncertainties are large. More evident is the case of the Sgr B2 complex (Minh et al. 1998), where the emission of HNCO appears to surround the C^{18}O emission which peaks toward the hot cores. While the HNCO abundance in Sgr B2(M) is 1×10^{-9} (a factor of 7 smaller than our measurements; Minh et al. 1998), it reaches values up to 1×10^{-8} in a position $2'$ north Sgr B2(M) ($28''$ away from our $20'', 100''$ position). Therefore the HNCO molecule seems to avoid the hot cores in massive star forming regions and most of its emission is observed to stem from the surrounding molecular gas envelope around the hot cores where, similar to that observed in GMCs (Sect 3.1), low velocity shocks would be responsible for the enhancement of HNCO emission (Flower et al. 1995). There are two exceptions in the sample

from Zinchenko et al. (2000), namely Orion-KL and Sgr A, which show larger abundances of HNC0, 8.7×10^{-9} and 6.3×10^{-9} , respectively. The abundance towards Sgr A is in agreement with our findings in the GC clouds, as this refers to a position $65''$ away from our source G–0.11 – 0.08. For the Orion-KL hot core, the difference in abundance might be related to the evolutionary state of this particular molecular core.

We have also observed that G–0.02 – 0.07 shows a relative low HNC0/ 13 CS abundance ratio. G–0.02 – 0.07, known as the $+50\text{km s}^{-1}$ cloud (Güsten et al. 1981), appears to be surrounding and interacting with Sgr A East, a supernova remnant located just behind the Galactic center (i.e. Zylka et al. 1990). Similar to what we observe in G+0.02 – 0.02 (Sect 3.2), the UV field associated with the high velocity shocks resulting from the supernovae interaction might be the responsible for the lower HNC0/ 13 CS abundance ratio observed in this source.

3.4. The origin of the large HNC0 abundance variation in the GC

The fractional abundance of HNC0 derived from the data presented in this work appear to be fairly constant in the typical Galactic center GMCs. This uniform abundance is significantly more evident when the HNC0/CS ratio is considered. As already mentioned above, the most likely origin of gas-phase HNC0 is via its ejection from dust grains by low velocity shocks erosion. Similar uniformity, within a factor of 4, is also found throughout the Galactic center region for the relative abundances of complex organic species ejected from grains (Requena-Torres et al. 2006, 2007).

However, we observe that the HNC0 abundances are strongly affected by the extreme physical processes present in hot molecular cores, supernova remnants and mainly photodissociation regions. With photodissociation rates almost twice as large as those of CH_3OH and slightly larger than those of NH_3 (Roberge et al. 1991), HNC0 seems to be the most sensitive molecule to the UV radiation fields, even more than NH_3 . Thus, while HNC0 survives in the gas-phase in the well shielded dense molecular clouds, it is almost completely wiped out in the unshielded regions of highly UV-irradiated clouds. This effect is also observed in the interfaces between supernovae shocks and the molecular environment, where the UV radiation generated in the hot plasma of the shock front is enough to photoionize and dissociate the molecular gas entering the shock.

This variation is clearly evident in the HNC0/CS ratio, not only due to the higher photodissociation energy of CS, but for the favored production of CS via ion reactions as a consequence of the mentioned enhanced abundance of S^+ in low UV-shielded regions ($A_v < 7$

Sternberg & Dalgarno 1995; Mauersberger et al. 2003).

Additionally, the HNC abundance is also affected to a lesser extent in dense star forming molecular cores. As noticed by Zinchenko et al. (2000), the HNC emission towards massive star forming cores does not show the high velocity wings observed in SiO, indicating that, though HNC is enhanced by low-velocity shocks, it is notoriously underabundant in the presence of high velocity shocks. Though Zinchenko et al. (2000) explain the low HNC abundance as a result of the destruction of O_2 (an important molecule in the pathways to gas-phase HNC formation) by the high velocity shocks, the low efficiency of HNC formation in gas-phase as well as its overall homogeneous abundance over the Galactic center region, seems to point to the destruction of the HNC molecule itself by fast shocks. The shock-induced UV field (Viti et al. 2002) might account for the dissociation of HNC in high velocity shocks.

3.5. From Galactic center to Galaxies

In the last years it has been recognized that the chemical complexity of the ISM in the nuclei of galaxies can be used to trace the processes which dominate their heating (Martín et al. 2006b). Rarer molecules like SiO, HCO and HOC^+ , which can be detected in nearby galaxies with different types of nuclear activity has been suggested to trace heating by PDRs and XDRs from Active Galactic Nuclei (AGN) like NGC1068 (Usero et al. 2004), or by shocks in Starburst Galaxies (SB) like NGC 253 (Martín et al. 2006b). Unfortunately, these lines are too weak to be detected beyond the more nearby galaxies.

In order to establish a chemical classification of the ISM in the nuclei of galaxies, that can be used out to moderate ($z \sim 1$) distances, and in the future even at higher redshift with ALMA, we need to identify the most suitable molecular tracers of the different dominating chemistries that also show strong emission lines. Diagnostic diagrams of line intensities of abundant molecules like HCN, HNC, HCO^+ , and CO have been proposed to discriminate between SB and AGN activity in Galaxies by Kohno et al. (1999); Kohno (2005); Aalto et al. (2007); Krips et al. (2007). It is claimed that the HCN/ HCO^+ line intensity ratio versus the HCN/CO line intensity ratio is a good discriminator between SB and AGN dominated nucleus.

The main drawbacks of the strong lines from very abundant molecules with high dipole moment like HCO^+ and HCN is that they can be severely affected by opacity effects (Martín-Pintado et al. 2008) and their line intensity ratios do not reflect the actual abundance ratios which are directly related to the chemistry. Further more the dynamic range of

line intensity ratios found in different types of galaxies are of only a factor $\lesssim 4$ (Kohno et al. 2007).

The results from this work point out that the relative abundance of HNCO seems to be one of the best discriminators between the chemistry driven by low velocity shocks found in SB like NGC253 and that driven by photodissociation due to the UV radiation from stellar clusters or AGNs. This molecule has the additional advantage to have transitions near those of C¹⁸O, allowing a precise determination of the fractional abundances, as well as reasonable intensities (of the order of C¹⁸O) for extragalactic studies. As an observability comparison with lines such as HCN, if we assume the luminosity of HNCO lines to be ~ 5 fainter than that of HCN(1 – 0) we estimate a luminosity of $L'_{HNCO} > 6 \times 10^8 L_{\odot}$ for ultraluminous infrared galaxies (ULIRGs, using the L'_{HCN}/L_{FIR} relation from Gao & Solomon 2004). For a ULIRG at $z=1$, we obtain an integrated intensity of $> 20 \text{ mJy km s}^{-1}$ observed 80 GHz. Assuming a linewidth of 200 km s^{-1} , line intensity would be $> 0.1 \text{ mJy}$. ALMA would detect this line at a 3σ detection level in 9 hours of time for a 100 km s^{-1} resolution.

Additionally, compared to other potentially good tracers of shock driven chemistry such as CH₃OH, which has been easily detected towards a number of starburst galaxies (Henkel et al. 1997) and recently also towards M 82 (Martín et al. 2006a), HNCO shows much simpler spectral features, which is fundamental when dealing with extragalactic broad line profiles with typical linewidths of a few hundred km s^{-1} , as well as a higher abundance contrast than CH₃OH.

In Fig. 5 we present a diagnostic diagram using the relative abundance of CS versus that of HNCO. We have used the ratio $^{12}\text{C}/^{13}\text{C} = 20$ (Wilson & Rood 1994) to calculate the CS abundances in the GC sources. The ratios show a very large dynamic range of up to 1.5 orders of magnitude. If we compare the GMCs and PDRs abundances, we observe a significant negative correlation between the HNCO and CS abundances as expected from the different origin of both molecules. This diagnostic plot shows a clear differentiation between sources with different types of chemistry. This abundance ratio diagram could be used as diagnostic to discriminate in extragalactic sources between the two main physical processes expected to be dominating in the chemistry of the ISM in SB galaxies and in AGN. The dashed lines in Fig. 5 have been traced perpendicular to the CS-HNCO correlation observed between GMCs and PDRs to guide the eye in the discrimination. AGNs, with a chemistry expected to be dominated by PDRs, would appear in the upper left corner while the non-UV irradiated material will be observed at the lower right corner with very high relative abundances of HNCO.

Unfortunately only a few galaxies have been measured in HNCO and all those measured correspond to starburst galaxies. We have added to the HNCO diagnostic diagram, the

abundance ratios derive for NGC 253, M 82, IC 342, NGC 4945, and Maffei 2. These data clearly show the differences in the heating and the chemistry of the molecular gas in each galaxy, closely related to the state of evolution of their nuclear starbursts. The upper limit to the HNC abundance of M 82 clearly locate this galaxy in the region of UV dominated material. This agrees well with the finding from other molecules like HCO towards this galaxy (García-Burillo et al. 2002) suggesting M 82 as the best case of late stage PDR dominated galaxy (Martín et al. 2006b). Surprisingly, the early state starbursts in NGC 253, assumed to be mainly dominated by shocks (Martín et al. 2003, 2005; Martín et al. 2006b), shows abundances of HNC within the range of the PDR region of the diagram, which suggest that a strong UV field is also affecting an important fraction of its molecular gas. Galaxies such as IC 342 and NGC 4945 show intermediate abundances suggesting an intermediate state of evolution as found in previous molecular studies (Wang et al. 2004; Meier & Turner 2005; Martín et al. 2006b), while Maffei 2 seems to be a source where PDRs have a lesser impact on the chemistry.

This diagnostic diagram should be considered complementary to similar efforts being carried out with HCN, HCO^+ and HNC and should be checked through observations of the HNC and CS emission in a sample of selected galactic nuclei with different types of activity. These observations are required to test the potential of the proposed CS vs HNC diagnostic diagram.

4. Conclusions

We have studied the HNC, ^{13}CS , C^{34}S , and C^{18}O emission towards 13 positions in the Central Molecular Zone in the Galactic center region. Column densities and excitation temperatures have been derived for each position. These set of sources represent a sample of the main different chemical processes affecting the molecular material.

With variations of up to a factor of 20 in abundance, the molecule of HNC is shown to be one of the most contrasted species among the observed sources. The derived HNC/ ^{13}CS abundance ratio shows particularly high contrast of up to a factor of 30 between sources. This ratio allows the grouping of the observed sources in three categories: 1) Giant Molecular Clouds showing a high HNC/ ^{13}CS ratio, 2) Photo dissociated regions and high velocity shocks interactions with the lowest observed ratios, and 3) hot molecular cores with intermediate HNC/ ^{13}CS ratios but with significantly higher H_2 column densities.

The negative correlation between the CS and HNC abundances relative to H_2 observed in these groups of sources support the idea of HNC being ejected from grain mantles by

low velocity shocks while CS formation is favored in PDRs environments via ion reactions.

We have used the results from the Galactic center sources as templates for the observed chemistry in extragalactic nuclei. Thus, we compared the observed abundances in the Galactic center with the available data on five starburst galaxies. A similarly large variation in the HNC abundance is observed with sources such as M 82 and NGC 253 showing abundances similar to the galactic PDRs while, on the other end, Maffei 2 appears to be more similar to the Galactic center GMCs. The CS vs HNC abundance diagram is suggested as a powerful tool to study the chemical differentiation in the nuclei of galaxies.

This work has been partially supported by the Spanish Ministerio de Educación y Ciencia under projects ESP2007-65812-C02-01 , ESP2004-00665, by the Comunidad de Madrid Government under PRICIT project S-0505/ESP-0237 (ASTROCAM), and by DGI Grant AYA 2005-07516-C02-01.

Facilities: IRAM 30m

REFERENCES

- Aalto, S., Spaans, M., Wiedner, M.C., & Hüttemeister, S. 2007, A&A, 464, 193
- Charnley, S.B., Kress, M.E., Tielens, A.G.G.M., & Millar, T.J. 1995, ApJ, 448, 232
- Dahmen, G., Hüttemeister, S., Wilson, T.L., et al. 1997, A&AS, 126, 197
- de Vicente, P., Martín-Pintado, J., Neri, R., & Colom, P. 2000, A&A, 361, 1058
- Drdla, K., Knapp, G. R., & van Dishoeck, E. F. 1989, ApJ, 345, 815
- Eisenhauer, F., Genzel, R., Alexander, T. et al. 2005, ApJ, 628, 246
- Figer, D.F.; McLean, I.S., & Morris, M. 1999, ApJ, 514, 202
- Flower, D.R., Pineau des Forêts, G., & Walmsley, C.M. 1995, A&A, 294, 815
- Frerking, M. A., Langer, W. D., & Wilson, R. W. 1982, ApJ, 262, 590
- Gao, Y., & Solomon, P. M. 2004, ApJS, 152, 63
- García-Burillo, S., Martín-Pintado, J., Fuente, A., Usero, A., & Neri, R. 2002, ApJ, 575, L55

- Ghez, A. M., Salim, S., Hornstein, S. D. 2005, *ApJ*, 620, 744
- Goicoechea, J. R.; Pety, J.; Gerin, M. et al. 2006, *A&A*, 456, 565
- Goldsmith, P. F., & Langer, W. D. 1999, *ApJ*, 517, 209
- Güsten, R., Walmsley, C.M., Pauls T. 1981, *A&A*, 103, 197
- Hasegawa, T. I., & Herbst, E. 1993, *MNRAS*, 263, 589
- Henkel, C., Jacq, T., Mauersberger, R., Menten, K.M., Steppe, H. 1997, *A&A*, 188, L1
- Hüttemeister, S., Wilson, T.L., Bania, T.M., & Martín-Pintado, J. 1993, *A&A*, 280, 255
- Hüttemeister, S., Dahmen, G., Mauersberger, R., Henkel, C., Wilson, T. L., & Martín-Pintado, J. 1998, *A&A*, 334, 646
- Iglesias, E. 1977, *ApJ*, 218, 697
- Jackson, J.M., Armstrong, J.T., Barrett, A.H. 1984, *ApJ*, 280, 608
- Jansen, D. J., Spaans, M., Hogerheijde, M. R., & Van Dishoeck, E. F. 1995, *A&A*, 303, 541
- Kohno, K., Matsushita, S., Vila-Vilaró, B., Okumura, S. K., Shibatsuka, T., Okiura, M., Ishizuki, S., & Kawabe, R. 2001, *ASP Conference Proceedings Vol. 249: “The Central Kiloparsec of Starbursts and AGN: The La Palma Connection”*, 672
- Kohno, K. 2005, *AIP conference proceedings 783 “The evolution of Starburst: The 331st Wilhelm and Else Heraeus Seminar”*, 203
- Kohno, K., Nakanishi, K., & Imanishi, M. 2007, *proceedings “The Central Engine of Active Galactic Nuclei”*, ed. L. C. Ho and J.-M. Wang, astro-ph/0704.2818
- Krabbe, A., Genzel, R., Eckart, A., & Najarro, F. 1995, *ApJ*, 447, L95
- Krips, M., Neri, R., García-Burillo, S., Combes, F., Martín, S., & Eckart, A. 2007, submitted
- Lindqvist, M., Sandqvist, A., Winnberg, A., Johansson, L.E.B., Nyman, & L.-A. 1995, *A&AS*, 113, 257L
- Martín, S., Mauersberger, R., Martín-Pintado, J., García-Burillo, S., & Henkel, C. 2003, *A&A*, 411, L465
- Martín, S., Martín-Pintado, J., Mauersberger, R., Henkel, C., & García-Burillo, S. 2005, *ApJ*, 620, 210

- Martín, S., Martín-Pintado, J., Mauersberger, R. 2006a, *A&A*, 450 L13
- Martín, S., Mauersberger, R., Martín-Pintado, J., & Henkel, C., García-Burillo, S. 2006b, *ApJS*, 164, 450
- Martín-Pintado, J., de Vicente, P., Fuente, A., & Planesas, P. 1997, *ApJ*, 482, 45
- Martín-Pintado, J., Rizzo, J.R., de Vicente, P., Rodríguez-Fernández, N.J., & Fuente, A. 2001, *ApJ*, 548, L65
- Martín-Pintado et al. 2008, in preparation
- Mauersberger, R., & Henkel, C. 1989, *A&A*, 223, 79
- Mauersberger, R., Henkel, C., Wilson, T.L., & Harju, J. 1989, *A&A*, 226, L5
- Mauersberger, R., Henkel, C., Weiß, A., Peck, A.B., Hagiwara, Y. 2003, *A&A*, 403, 561
- McQuinn, K.B.W., Simon, R., Law, C.J. et al. 2002, *ApJ*, 576, 274
- Meier, D.S & Turner, J.L. 2005, *ApJ*, 618, 259
- Millar, T.J., Herbst, E., & Charnley, S.B. 1991, *ApJ*, 369, 147
- Minh, Y.C., Haikala, L., Hjalmarson, Å., & Irvine, W. M. 1998, *ApJ*, 498, 261
- Minh, Y.C., Kim, S.-J., Pak, S., Lee, S., Irvine, W. M., Nyman, L.-Å. 2005, *New Astronomy*, 10, 425
- Minh, Y.C. & Irvine, W.M. 2006, *New Astronomy*, 11, 594
- Morris, M. & Serabyn, E. 1996, *ARA&A*, 34, 645
- Novozamsky, J.H., Schutte, W.A., & Keane, J.V. 2001, *A&A*, 379, 588
- Oka, T., Hasegawa, T., Sato, F., Tsuboi, M., Miyazaki, A. 1998, *ApJS*, 118, 455
- Oka, T., White, G.J., Hasegawa, T., Sato, F., Tsuboi, M., Miyazaki, A. 1999, *ApJ*, 515, 249
- Requena-Torres, M.A., Martín-Pintado, J., Rodríguez-Franco, A, et al. 2006, *A&A*, 455, 971
- Requena-Torres, Martín-Pintado, J., Martín, S., Morris, M. 2007, *ApJ* Accepted
- Roberge, W.G., Jones, D., Lepp, S., Dalgarno, A. 1991, *ApJS*, 77, 287
- Rodríguez-Fernández, N.J., Martín-Pintado, J., & de Vicente, P. 2001, *A&A*, 377, 631

- Serabyn, E. & Güsten, R. 1991, *A&A*, 242, 376
- Shull, J. M., & McKee, C. F. 1979, *ApJ*, 227
- Sidoli, L.; Mereghetti, S.; Treves, A.; Parmar, A. N.; Turolla, R.; Favata, F. 2001, *A&aA*, 372, 651
- Sternberg, A., & Dalgarno, A. 1995, *ApJS*, 99, 565
- Turner, B.E., Terzieva, R., & Herbst, E. 1999, *ApJ*, 518, 699
- Usero, A., García-Burillo, S., Fuente, A., Martín-Pintado, J., & Rodríguez-Fernández, N. J. 2004, *A&A*, 419, 897
- Viti, S., Natarajan, S., & Williams, D.A. 2002, *MNRAS*, 336, 797
- Wang, M., Henkel, C., Chin, Y.-N., Whiteoak, J. B., Hunt Cunningham, M., Mauersberger, R., & Muders, D. 2004, *A&A*, 422, 883
- Wilson, T. L., & Rood, R. T. 1994, *ARAA*, 32, 191
- Zinchenko, I., Henkel, C., & Mao, R.Q. 2000, *A&A*, 361, 1079
- Zylka, R., Mezger, P.G., Wink, J.E. 1990, *A&A*, 234, 133

Table 1: Coordinates and location of observed sources

Source	α_{J2000}	δ_{J2000}	Region
Sgr B2M	17 ^h 47 ^m 20 ^s .4	–28°23′07″	Sgr B
Sgr B2M(20″, 100″)	17 ^h 47 ^m 21 ^s .9	–28°21′27″	Sgr B
Sgr B2M(–40″, 0″)	17 ^h 47 ^m 17 ^s .4	–28°23′07″	Sgr B
Sgr B2M(20″, –180″)	17 ^h 47 ^m 21 ^s .9	–28°26′07″	Sgr B
Sgr B2S	17 ^h 47 ^m 20 ^s .5	–28°23′45″	Sgr B
Sgr B2N	17 ^h 47 ^m 20 ^s .3	–28°22′19″	Sgr B
G+0.24 + 0.01	17 ^h 46 ^m 09 ^s .8	–28°43′42″	Dust Ridge
G–0.11 – 0.08	17 ^h 45 ^m 38 ^s .8	–29°04′05″	Sgr A
G+0.83 – 0.18	17 ^h 48 ^m 16 ^s .6	–28°19′17″	Sgr B
G–0.02 – 0.07	17 ^h 45 ^m 50 ^s .6	–28°59′09″	Sgr A
Sgr A* ^a	17 ^h 45 ^m 37 ^s .7	–29°00′58″	Sgr A
G+0.02 – 0.02	17 ^h 45 ^m 42 ^s .8	–28°55′51″	Sgr A
G+0.18 – 0.04	17 ^h 46 ^m 11 ^s .3	–28°48′22″	The Sickle

^aThe position observed in this work correspond to the offset (–30″, –30″) relative to the nominal position of Sgr A*.

Table 2. Integrated intensity derived for the observed transitions of C¹⁸O, C³⁴S and ¹³CS

SOURCE	V _{LSR} (km s ⁻¹)	C ¹⁸ O		C ³⁴ S		¹³ CS
		1 – 0	2 – 1	3 – 2	5 – 4	3 – 2
		109.782	219.560	144.617	241.016	138.739
Sgr B2M	60	70 (1)	128 (2)	56 (2)	50 (10)	40 (1)
(20'', 100'')	67	27 (1)	32 (1)	14.3 (0.8)	6.6(0.9)	8.6(0.5)
(-40'', 0'')	54	7 (1)	14 (2)	25 (1)	7.2 (0.6)	8.4 (1.2)
	71*	48 (1)	72 (3)	12.1(1.7)
(20'', -180'')	50	9.7 (0.6)	12 (3)	5.2 (0.6)	< 0.6	3.4 (0.5)
	65*	6.7 (0.8)	11 (4)
Sgr B2S	61	52 (1)	87 (1)	27.9 (0.7)	13.5 (1.5)	17.6 (0.6)
	92*	4.8 (0.8)	4.4 (0.7)
Sgr B2N	63	65 (2)	81 (1)	21 (1)	...	48 (8)
Sgr A*	20	15.8 (0.6)	24 (3)	16.0 (1.3)	8 (2)	10.4 (0.6)
G + 0.02 – 0.02	-13	19.7 (0.4)	26 (3)	8.6 (0.6)	1.5 (0.8)	4.0 (0.4)
	90	11.5 (0.3)	21 (3)	7.4 (0.6)	3.8 (0.8)	6.0 (0.5)
G + 0.24 + 0.01	34	17.6 (1.0)	22.8 (1.7)	7.9 (0.6)	< 1.6	4.8 (0.2)
G – 0.11 – 0.08	17	14.9 (0.5)	23.0 (1.0)	7.8 (0.3)	2.0 (0.5)	6.1 (0.4)
	54*	4.2 (0.7)	4.4 (1.1)
G + 0.83 – 0.18	38	16.0 (0.5)	15.4 (0.6)	2.8 (0.5)	1.5 (0.2)	3.0 (0.3)
G – 0.02 – 0.07	51	32.5 (1.2)	46.8 (1.5)	25.5 (0.6)	11.7 (0.7)	16.6 (0.5)
G + 0.18 – 0.04	21	6.9 (0.6)	9.7 (1.8)	< 1.1	< 0.8	2.6 (0.6)
	72	6.3 (0.6)	8.5 (1.8)	< 2.2	< 1.6	3.4 (0.8)

Note. — Integrated intensities in T_A^* scale (K km s⁻¹). Quantum numbers and frequencies (GHz) are given for each transition. Different entries for a source indicate resolved velocity components. The velocity components with * do not show HNC0 emission.

Table 3. Integrated intensity derived for the observed transitions of HNC0

SOURCE	5 _{0,5} – 4 _{0,4} 109.905	6 _{1,6} – 5 _{1,5} 131.394	6 _{0,6} – 5 _{0,5} 131.885	6 _{1,5} – 5 _{1,4} 132.356	7 _{1,7} – 6 _{1,6} 153.291	7 _{0,7} – 6 _{0,6} 153.865	7 _{1,6} – 6 _{1,5} 154.414
Sgr B2M	64.3 (1.4)	13.7 (0.8)	76.8 (0.8)	11.3 (0.9)	18.0 (0.8)	72.3 (1.4)	18.9 (1.6)
(20'', 100'')	227.2 (0.8)	6.2 (1.7)	226.0 (1.2)	4.5 (1.0)	8.1 (0.4)	160 (3)	4.2 (0.4)
(–40'', 0'')	204.4 (0.5)	14.0 (1.1)	201.1 (1.4)	10.4 (1.4)	14.2 (0.8)	194.4 (1.3)	11.3 (0.8)
(20'', –180'')	86.2 (0.2)	1.0 (0.3)	75.2 (1.7)	1.7 (0.3)	3.3 (0.3)	70.4 (0.5)	...
Sgr B2N	132 (5)	20 (2)	112 (3)	18.4 (1.6)	65.6 (1.6)	111 (4)	36 (5)
Sgr B2S	95.2 (0.4)	6 (2)	120.6 (1.0)	6.4 (0.8)	9.9 (0.4)	107 (2)	10.8 (0.5)
Sgr A*	5.4 (0.6)	...	6.9 (1.4)	7.2 (0.7)	...
G + 0.02 – 0.02	8.0 (0.3)	...	9.3 (0.6)	3.3 (0.3)	...
	6.8 (0.3)	...	8.1 (0.6)	3.2 ^a	...
G + 0.24 + 0.01	76.8 (0.2)	...	78.3 (0.8)	...	2.1 (0.3)	45 (2)	...
G – 0.11 – 0.08	116.9 (0.2)	...	112.0 (0.9)	...	1.8 (0.2)	76 (2)	0.6 (0.2)
G + 0.83 – 0.18	64.3 (0.3)	...	45.8 (0.6)	26.1 (0.8)	0.6 (0.2)
G – 0.02 – 0.07	93.9 (0.2)	...	89.8 (1.4)	1.5 (0.2)	...	56 (2)	...
G + 0.18 – 0.04	1.6 (0.2)	2.3 (0.3)	...
	7.4 (0.2)	...	3.1 (0.8)	2.0 (0.2)	...
	8 _{1,8} – 7 _{1,7} 175.189	10 _{2,k'} – 9 _{2,k'} 219.733	10 _{0,10} – 9 _{0,9} 219.798	11 _{1,11} – 10 _{1,10} 240.876	11 _{1,10} – 10 _{1,9} 242.639	12 _{2,k'} – 11 _{2,k'} 263.672	12 _{0,12} – 11 _{0,11} 263.748
Sgr B2M	31 (5)	7.1 (1.2)	40 (2)	16 (2)	43.5 (1.8)	22 (9)	57.3 (1.5)
(20'', 100'')	6.8 (0.4)	...	48 (4)	...	0.9 (0.3)	...	16.4 (0.6)
(–40'', 0'')	14.1 (0.7)	4.1 (0.5)	94.1 (1.3)	6.6 (0.6)	4.7 (0.2)	...	44.5 (1.1)
(20'', –180'')	1.5 (0.1)	...	17.3 (0.5)	14.4 (1.1)
Sgr B2N	49 (2)	22 (4)	45 (2)	66 (6)	22 (3)	49 (4)	81.2 (1.7)
Sgr B2S	11.0 (0.3)	1.9 (1.0)	63.2 (1.0)	7.5 (0.6)	9.7 (1.1)	1.6 (0.5)	43 (3)
G + 0.24 + 0.01	1.3 (0.3)	...	10.6 (0.6)
G – 0.11 – 0.08	1.2 (0.3)	...	13.8 (0.6)
G + 0.83 – 0.18	3.3 (0.5)
G – 0.02 – 0.07	2.8 (0.3)	...	14.8 (1.2)

Note. — See Fig. 2.

^aEstimated contamination due to low velocity CH₃C₂H emission subtracted from fitted profile.

Table 4: Derived column densities and rotational temperatures

Source	C ¹⁸ O		C ³⁴ S		¹³ CS ^a	HNCO	
	($\times 10^{15} \text{cm}^{-2}$)	(K)	($\times 10^{13} \text{cm}^{-2}$)	(K)	($\times 10^{13} \text{cm}^{-2}$)	($\times 10^{14} \text{cm}^{-2}$)	(K)
Sgr B2M	73(2)	13.4(0.3)	19(4)	18(3)	9.4(0.4)	13.0(0.3)	39(0.4)
Sgr B2M(20'', 100'')	23(2)	8.7(0.4)	5.0(0.7)	12.0(1.0)	3.2(0.2)	26(2)	14.8(0.1)
Sgr B2M(-40'', 0'')	50(3)	10.7(0.5)	9.1(0.9)	9.2(0.4)	7.6(0.8)	24(2)	19.0(0.1)
Sgr B2M(20'', -180'')	8.1(1.9)	11(3)	1.9(0.0)	10 ^a	1.2(0.2)	10(1)	14.8(0.1)
Sgr B2N	54(2)	9.0(0.2)	7.5(0.4)	10 ^a	17(3)	23.2(0.7)	55.6(0.9)
Sgr B2S	50(2)	12.2(0.3)	9.4(1.0)	11.9(0.8)	6.5(0.2)	13.1(0.2)	22.6(0.1)
G+0.24 + 0.01	15(1)	9.4(0.8)	3.5(0.2)	10 ^a	1.8(0.1)	8.6(0.2)	13.9(0.2)
G-0.11 - 0.08	14(1)	11.0(0.7)	3.0(0.6)	8.6(0.9)	2.2(0.2)	13.0(0.2)	12.6(0.1)
G+0.83 - 0.18	12(7)	7.4(0.3)	1.1(0.3)	12.4(1.5)	1.1(0.2)	7.8(0.3)	9.1(0.1)
G-0.02 - 0.07	29(2)	10.3(0.5)	8.7(0.5)	11.6(0.4)	6.1(0.2)	10.5(0.2)	13.6(0.2)
Sgr A*	14(2)	10.8(1.3)	5.4(1.5)	12(2)	3.8(0.2)	1.1(0.6)	35(12)
G+0.02 - 0.02	17(2)	9.3(0.8)	3.4(1.5)	7.6(1.5)	1.5(0.2)	0.96(0.15)	10.5(0.7)
	11(2)	13(2)	2.5(0.6)	12.2(1.7)	2.2(0.2)	0.83(0.14)	10.5(0.7)
G+0.18 - 0.04	6.1(1.4)	10(2)	< 0.4	10 ^a	1.0(0.2)	0.42(0.16)	46(29)
	5.7(1.4)	10(2)	< 0.8	10 ^a	1.2(0.2)	1.1(0.2)	6.9(0.4)

^a T_{ex} value fixed to 10 K.

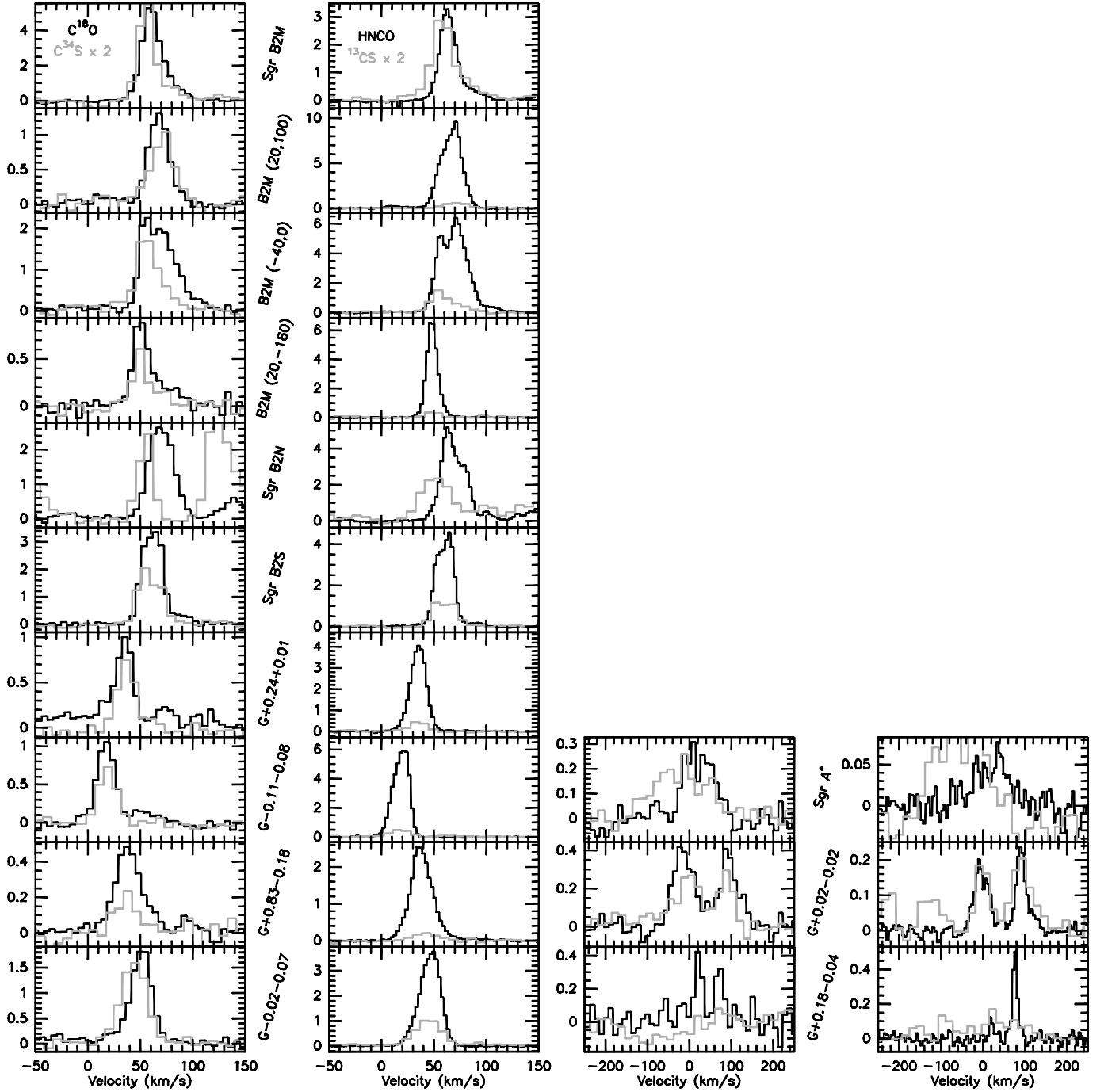


Fig. 1.— Sample spectra of the brightest transitions of each observed molecule, namely $\text{C}^{18}\text{O}(2-1)$, $\text{C}^{34}\text{S}(3-2)$, $\text{HNC}(5_{0,5}-4_{0,4})$ and $^{13}\text{CS}(3-2)$. The source identification is shown between the two spectra. The intensity of $\text{C}^{34}\text{S}(3-2)$ and $^{13}\text{CS}(3-2)$ has been multiplied by a factor of two for the sake of clarity. Temperature scale is T_{A}^* (K).

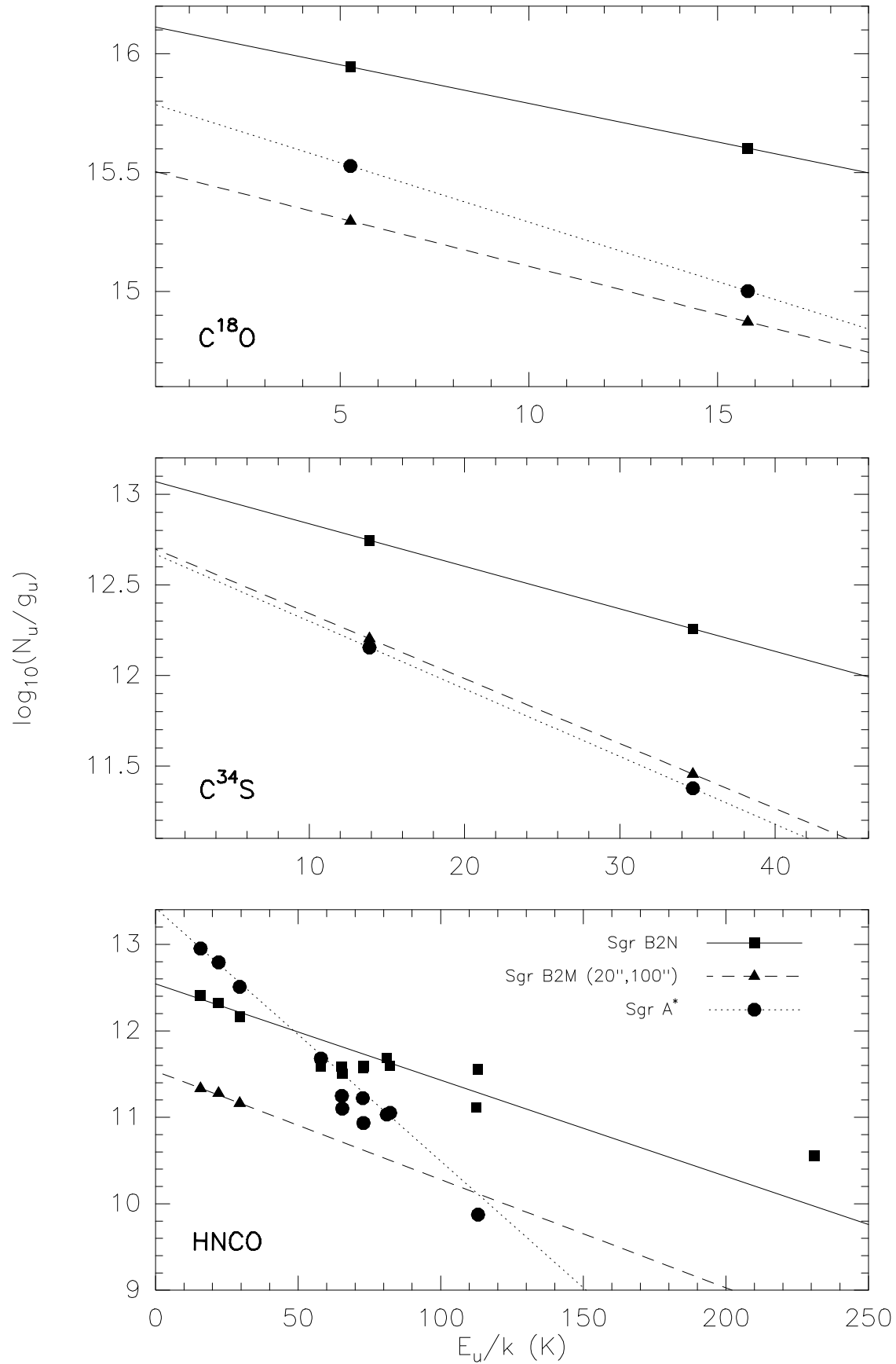


Fig. 2.— Sample of rotational diagrams derived from $C^{18}O$, $C^{34}S$ and HNC0 in three selected representative sources.

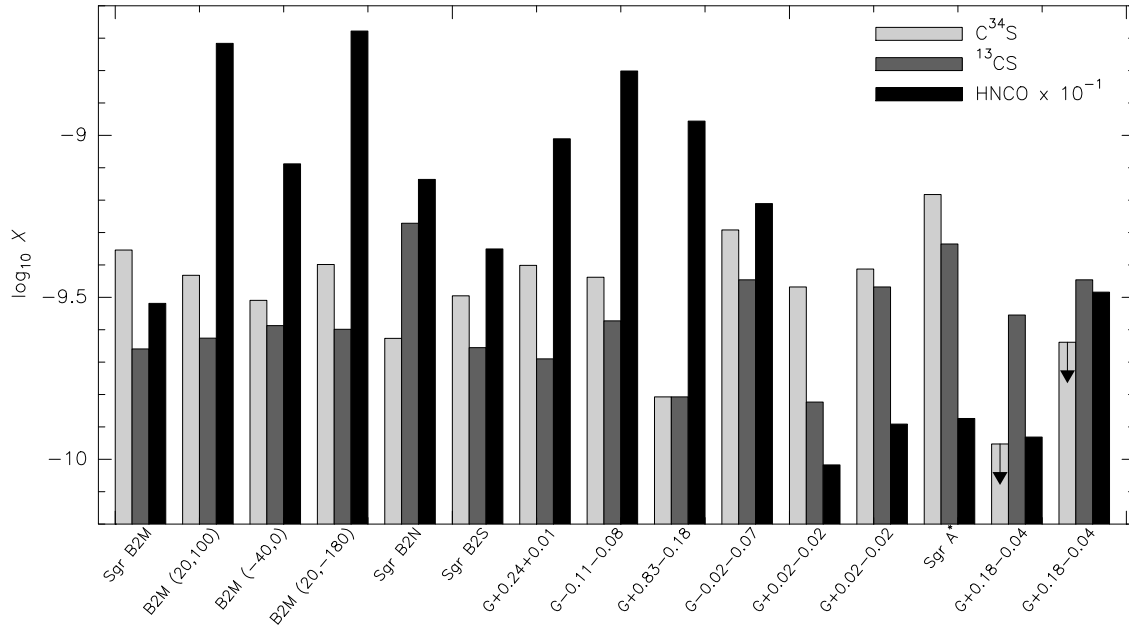


Fig. 3.— Fractional abundances relative to H_2 assuming a conversion factor of $C^{18}O/H_2 = 1.7 \times 10^{-7}$ (Frerking et al. 1982). Arrows represent upper limits to the observed abundances.

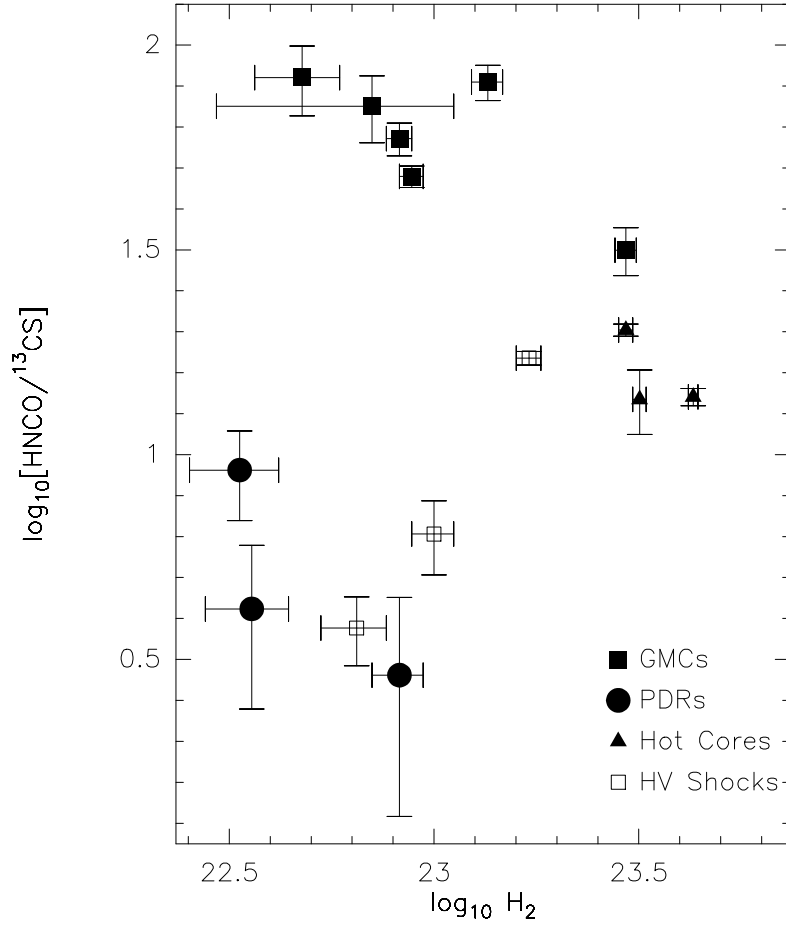


Fig. 4.— Relative abundance ratio HNCO/¹³CS versus H₂ column density ($\text{C}^{18}\text{O}/\text{H}_2 = 1.7 \times 10^{-7}$, Frerking et al. 1982) in logarithmic scale for the sample of sources observed in the Galactic center. The different symbols represent the PDR clouds, GC giant molecular clouds, hot cores, and sources affected by high velocity shocks.

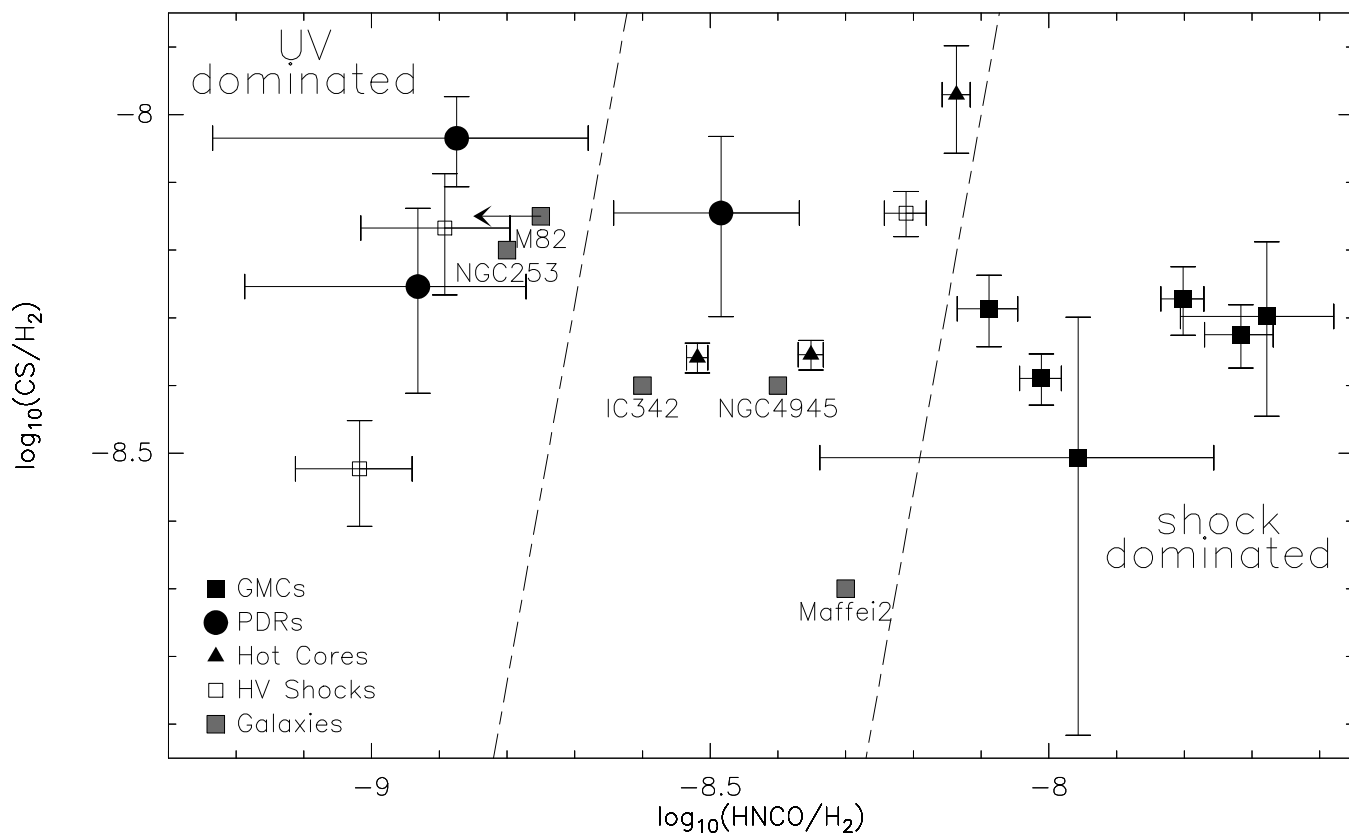


Fig. 5.— Proposed diagnostic diagram. The abundance relative to H_2 of CS versus that of HNCO in logarithmic scale for the sample of sources observed in the Galactic center. Symbols are as in Fig. 4. The diagram has the potential to discriminate between the UV (PDR, upper left corner) and shocks (GMCs, lower right) dominating the ISM in the nuclei of galaxies. Available data towards five starburst galaxies are represented by grey filled squares, where the upper HNCO detection limit towards M82 is represented with an arrow (see Table 7 in Martín et al. 2006b, for references). Additional details on this plot are explained in the text.